Impact performance of RC piers protected by closed-cell aluminium foam (CAF) of different thicknesses
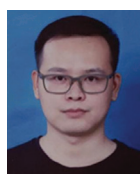
Authors:

[1] **Jingdong Liu**, MCE
ljd3477@163.com

[1] **Benying Wu**, MCE
wubenying163@163.com
Corresponding author

[1] Prof. **Xiwu Zhou**
408680014@qq.com

[1] **Bo Wang**, MCE
BoWang1127@qq.com

[2] **Wenchao Zhang**, PhD. CE
1350392000@qq.com

[1] Foshan University, Foshan, China
School of Transportation, Civil Engineering and
Architecture
[2] Tongji University, Shanghai, China
Bridge Engineering Department

Research Paper

Jingdong Liu, Benying Wu, Xiwu Zhou, Bo Wang, Wenchao Zhang

Impact performance of RC piers protected by closed-cell aluminium foam (CAF) of different thicknesses

Considering ship–bridge collisions can cause serious damage to pier components, we investigated the protective effect of closed-cell aluminium foam (CAF) on reinforced concrete (RC) piers. The effect of CAFs with different thicknesses on the impact resistance of RC pier specimens was studied by analysing the impact force, displacement, reinforcement strain, other dynamic responses of RC pier specimens, and the damage degree of RC piers using an ultrahigh drop hammer impact test system. The results show that the CAF material was in a linear elastic stage when the impact velocity was within 0.76 to 1.14 m/s. When the thicknesses were increased from 50 mm to 75 mm and 100 mm, the impact force and top displacements tested from the two groups of specimens showed an increasing amount of decline. The CAF material was observed to be at a yield platform stage when the value of the impact velocity was within 1.14 to 1.98 m/s. Under these conditions, the CAF material exhibited the best energy consumption and absorbed the impact energy in a nearly constant stress stage, while the impact force remained approximately constant. This study discovered that under high-energy impact conditions, CAF materials with larger thicknesses delayed entry into the densification stage, resulting in better control of the lateral dynamic responses of RC piers.

Key words:

bridge structure, collision prevention, closed-cell aluminium foam (ACF), horizontal impact, crashworthiness

Prethodno priopćenje

Jingdong Liu, Benying Wu, Xiwu Zhou, Bo Wang, Wenchao Zhang

Ponašanje AB stupova zaštićenih aluminijskom pjenom zatvorenih ćelija (CAF) različitih debljina u slučaju udara

S obzirom na to da sudari brodova u mostove mogu uzrokovati ozbiljna oštećenosti dijelova stupa, u radu je istražen zaštitni učinak aluminijske pjene zatvorenih ćelija (CAF) na armiranobetonskim (AB) stupovima. Ispitivan je utjecaj CAF-a različitih debljina na otpornost na udare uzoraka AB stupa analizirajući udarnu silu, pomak, deformaciju armature, ostale dinamičke odzive uzoraka AB stupa, te razinu oštećenosti AB stupova pomoću ultravisokog sustava za ispitivanje udarom čekića. Rezultati pokazuju da je materijal CAF-a bio u linearnoj elastičnoj fazi kada je brzina udara bila unutar 0,76 do 1,14 m/s. Kada su debljine povećane s 50 mm na 75 mm i 100 mm, udarna sila i pomaci testirani iz dvije skupine uzoraka pokazali su sve veći pad. Materijal CAF-a promatran je u fazi popuštanja kada je vrijednost brzine udara bila unutar 1,14 do 1,98 m/s. U tim je uvjetima materijal CAF-a pokazao najbolju potrošnju energije i apsorbirao udarnu energiju u gotovo stalnoj fazi naprezanja, a udarna je sila ostala približno konstantna. U ovom istraživanju otkriveno je da u uvjetima visokog energetskog udara, materijali CAF-a s većim debljinama odgađaju ulazak u fazu očvršćivanja što rezultira boljom kontrolom lateralnih dinamičkih odziva AB stupova.

Ključne riječi:

konstrukcija mosta, sprječavanje sudara, aluminijska pjena zatvorenih ćelija (CAF), horizontalni udar, otpornost na udare

1. Introduction

The rapid development of the economy and trade in recent years has resulted in increased ship transportation and cargo throughput processes, accompanied by an increase in the number of ship–bridge collisions, resulting in financial losses and casualties [1-3]. The impact resistance of reinforced concrete (RC) piers is an important indicator of the overall safety performance of bridges owing to their bearing functions during bridge construction [4-6]. Although several researchers have improved and tested bridges and other building structures to reduce the damage caused by vehicle and ship collisions [7-11], protecting structures using additional protective materials is more convenient [12]. The anti-collision properties of closed-cell aluminium foams (CAFs) have attracted considerable attention from researchers because of their capacity to absorb more impact energy, extend the collision time of ships through buffering and energy dissipation, reduce the impact force on ships, and effectively protect the safety of both piers and ships [13-15].

As new engineering materials, CAFs exhibit many excellent properties owing to their unique structure. Currently, most studies in China and internationally regarding CAF have focused on experimental evaluations of their static and dynamic mechanical properties. According to these studies, the compression process of CAF materials progresses through three distinct stages: linear elastic, plastic platform, and densification stages [16, 17]. Observation of these three stages revealed high and wide platforms in the uniaxial compression experiments of CAF, with considerable energy absorbed under constant stress states during the compression processes. Energy consumption capacity has been found to increase with the extension of this platform [18-20]. In experimental compression-shear tests of CAF under quasi-static conditions, Xueyan et al. [21] observed that an increase in the pore size of CAF increased the yield stress under the same density conditions. Shakibanezhad et al. [22] conducted quasi-static compression tests on low-, medium-, and high-density aluminium foams and found that with an increase in foam density, the dense strain decreased, whereas other mechanical properties (such as elastic modulus, yield stress, platform stress, and energy absorption capacity) increased. Li et al. [23] studied the mechanical behaviour of CAF under biaxial loading and conducted shear-compression coupling tests by changing the loading angle. The results indicated that CAF under biaxial coupling loading exhibits strong yield stress and that the density of CAF significantly affects its mechanical properties under compression and shear.

Studies on the static mechanical properties of CAF show that CAF are ideal plastic energy dissipation buffer materials with high energy absorption efficiencies and suitable plastic crushing forces, thus highlighting the possibility of applying CAF in the impact protection field of bridge piers.

The dynamic mechanical properties of CAF determine the scope and depth of their applications in practical engineering. In previous studies on the combination of CAF and reinforced concrete members, CAF showed excellent cushioning performance.

Binchao et al. [24] studied the dynamic compression properties and low-speed impact resistance of CAF materials. The results revealed that the impact cushioning effect of the high-porosity CAF was evident, and the deformation morphology was similar to that of quasi-static deformations. Sun et al. [25-28] investigated the behaviour of aluminium foam sandwich panels under both low-speed and explosive impact conditions. The results indicated that the changes in the material were highly sensitive to the strength of the impact and the lamination and gradients of the aluminium foam cores. This study also observed that the density gradients of the CAF sandwich panels significantly influenced the CAF sandwich panel deformations, energy absorption capacities, and failure degrees. Liu et al. [29] studied the anti-explosion performance of steel wire mesh and CAF-reinforced composite walls. The results showed that the failures and lateral displacements of high-performance composite walls reinforced with CAF were reduced under explosive impact loads to varying degrees. Xia et al. [30] conducted experimental tests on the protective effects of CAF materials with different density gradients on a concrete slab. The results showed that increasing the density gradient could improve the anti-explosion properties of the aluminium foam material while decreasing the density gradient tended to reduce the effectiveness of the aluminium foam material. Lin et al. [31] studied the anti-explosion performance of RC slabs protected by CAF, finding that the anti-explosion performance of the concrete slabs was promoted by the increases in the thicknesses of the CAF material. Cong et al. [32] investigated protection measures for RC columns under collision impact loading and determined that the damage to structural columns with the protection of CAF was less than the damage to structural columns without protection. Ying et al. [33] examined the damage effects of concrete slabs when aluminium foam protection layers were available or unavailable. Increasing the thickness of the protective layer of the CAF proved to be an effective method to reduce the deflection deformations of the examined RC slabs as well as the degree of damage. Yong et al. [34] proposed a CAF filling structure to protect bridge piers from the high risk of rolling-stone impact loading. Wu et al. [35] used pendulum tests and finite element analysis methods to conduct comparative experimental research on bridge pier anti-collision devices incorporating CAF of different thicknesses and structural formations. The results of the aforementioned study confirmed that the special structural characteristics of the CAF material had clear protective effects in the case of a single impact on bridge piers. Dongfeng [36] conducted pendulum impact tests on bridge piers protected by CAF protection devices and analysed the influence law of the effects of CAF materials on RC piers.

Although abundant research has been conducted on the dynamic material properties of CAF and their combination with concrete structures, studies on applying CAF in the collision avoidance of RC bridge piers remain limited. Experiments simulating ship collisions through the transverse impact of a trolley are also relatively lacking. Previous studies have indicated that a change in the impact conditions could easily affect the impact resistance performance of CAF on piers [37, 38], with horizontal impact

tests conducted to address this problem. Starting from the impact condition and influence of the CAF thickness change, the influence of each parameter change on the dynamic response of the piers under impact was analysed.

2. Overview of the testing processes

2.1. Parameters of test specimens

The testing processes of this study were based on a comparative experimental method, with a cylindrical pier used as a prototype to design and construct six pier-scale models in two groups in a proportion of 1:5, according to the principle of similarity. To ensure the accuracy of the test results, three different thicknesses of the CAF material with two different volume densities were used for the impact protection of the two groups of RC piers.
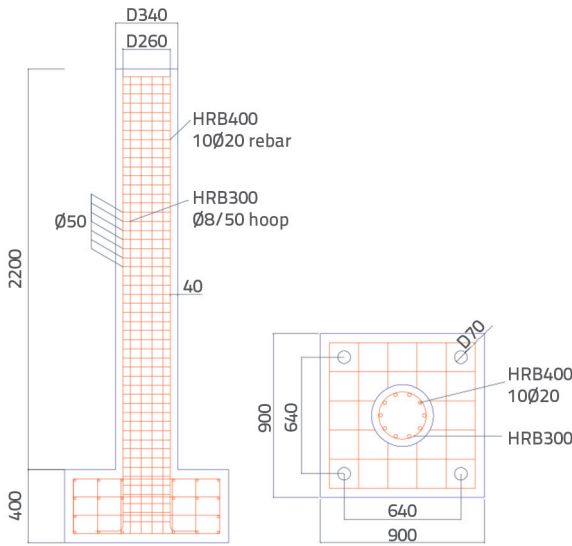

Figure 1. Schematic diagram of the specimen (unit: mm)

The pier models, made using C40 concrete, had column section diameters of 340 mm and heights of 2,200 mm. Longitudinal reinforcements were made of hot-rolled ribbed steel bars with a yield strength of 400 MPa (HRB400); ten longitudinal reinforcements were applied to each pier model. The longitudinal reinforcements were symmetrically reinforced in the direction

of the circular section. The stirrups were Grade I common reinforcements with a yield strength of 300 MPa (HPB300) and a diameter of 8 mm. A welding construction method was used to connect the reinforcements. Figure 1 illustrates the reinforcement of the one-pier model, while Figure 2 details the selected CAF materials used for the tests.

The CAF material was manufactured by Christie Foam Metal Co., LTD (Suzhou, China) (Figure 2). To study the compressive mechanical properties of CAF, two kinds of CAF with densities of 0.55 g/cm³ and 0.65 g/cm³ were selected for uniaxial compression tests. The testing machine is shown in Figure 3. The stress-strain curves obtained from the tests are shown in Figure 4. For convenience, the loading direction of the CAF in a later description is specified here, which by default is the same as the direction in which the thickness changes.

Figure 2. CAF protective materials with different thicknesses

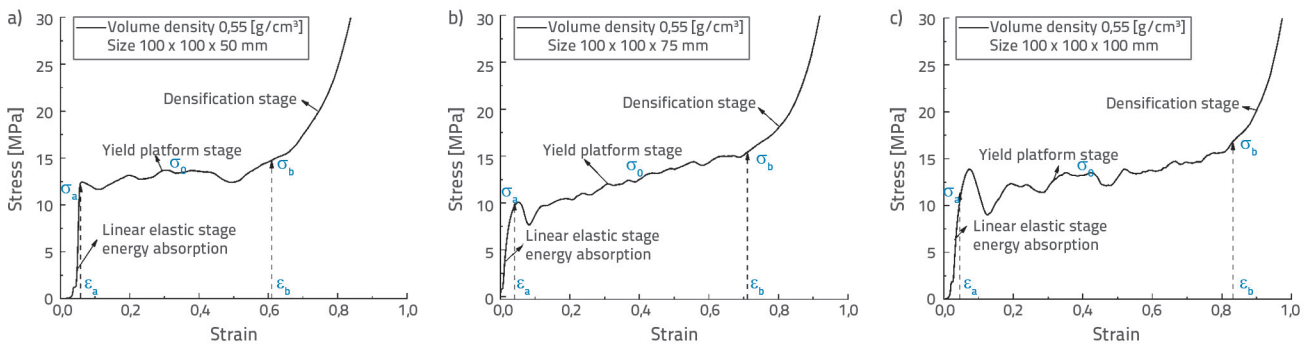**Figure 3. Compression tests of the CAF material**

Figure 4. Compressive stress–strain curves of the CAF material. Sizes: a) 100 × 100 × 50 mm; b) 100 × 100 × 75 mm; c) 100 × 100 × 100 mm

Table 1. Design parameters of the CAF materials

Material No.	Volume density [g/cm³]	Dimension [mm]	Yield platform stress [MPa]	Densification strain	Energy absorption [J]
A1	0.55	210×100×50	12.87	0.40	7285
A2	0.55	210×100×75	12.92	0.65	10927
A3	0.55	210×100×100	12.65	0.82	14570
A4	0.65	210×100×50	17.34	0.36	10478
A5	0.65	210×100×75	17.64	0.66	15717
A6	0.65	210×100×100	17.87	0.84	20956

Table 2. Reinforcement material properties

Reinforcement category	Reinforcement diameter [mm]	Yield strength [MPa]	Ultimate strength [MPa]	Elastic modulus E [MPa]
HRB400	20	486	640	$2.00×10^5$

Table 3. Concrete mechanical properties

Concrete grade	VCompressive strength value [MPa]	Elastic modulus E [MPa]
C40	44.83	$3.28×10^4$

Table 4. Model design parameters

Group	Specimen No.	Longitudinal reinforcement HRB400	Stirrup HPB300	Strength grade of the concrete	CAF No. used for the specimen
1st group	Z1-20	10Ø20	Ø8/50	C40	A1
	Z2-20	10Ø20	Ø8/50	C40	A2
	Z3-20	10Ø20	Ø8/50	C40	A3
2nd group	Z4-20	10Ø20	Ø8/50	C40	A4
	Z5-20	10Ø20	Ø8/50	C40	A5
	Z6-20	10Ø20	Ø8/50	C40	A6

As seen in Figure 4, the yield platform stress remained approximately unchanged when the thicknesses of the CAF material increased from 50 mm to 75 mm and 100 mm. However, the lengths of the yield platforms were slightly increased, along with an increase in the densification strain. When the CAF thickness was raised to 100 mm, the densification stage showed a slower growth tendency when compared to the densification stages at 50 mm and 75 mm CAF thicknesses. The work **W** done by the deformations and the yield platform stress σ_0 were obtained according to the stress–strain values [39]:

$$W = \int_0^{\varepsilon_b} \sigma(\varepsilon)d\varepsilon \tag{1}$$

Where **W** represents the work absorbed during the deformation of the CAF material, σ indicates the low stress of the CAF material, and ε_b represents the flow strain of the CAF material.

$$\sigma_0 = \frac{\int_{\varepsilon_a}^{\varepsilon_b} \sigma(\varepsilon)d\varepsilon}{\varepsilon_b - \varepsilon_a} \tag{2}$$

where σ_0 represents the yield platform stress, σ_a denotes the yield stress, ε_a indicates the yield strain, and ε_b indicates the strain of the CAF in the densification stage.

Based on the present study, the parameters of the CAF material were determined using Equations (1) and (2) and are listed in Table 1.

The reinforcements selected for the test were sampled and loaded on an electro-hydraulic servo universal testing machine to obtain the properties of the reinforcement materials, such as the yield strength and ultimate strength values, as listed in Table 2.

Simultaneously, a total of twelve testing cubes (150 × 150 × 150 mm) were prepared as per experimental requirements to conduct compressive tests of the specimens. The mechanical properties of concrete are listed in Table 3, while the model design parameters are listed in Table 4.

2.2. Device of the test

The test loading device used in this study was a multifunctional ultrahigh-drop hammer impact test system. The testing machine

system comprised a vertical falling hammer and a horizontal small boat model (Figure 5). The principle of the testing device was to change the drop hammer heights and counterweights to adjust the impact energy of the boat model and then use the free-falling body of the drop hammer to drag the boat model horizontally to collide with the pier models along a set track. The drop hammer was raised to a maximum height of 18 m, and its weight ranged from 166 kg to 1,500 kg. In addition, the weight of the impact boat model was 1,200 kg, while the weight of the boat model could be changed using a counterweight. The designed counterweight of the drop hammer was 216 kg in this study. The rigid bow of the impacting boat model was fixed with the CAF material, as shown in Figure 6. With a laser speed-measuring system installed at the end of a fixed track, the impact values of the instantaneous velocity can be measured accurately. The boat model's impact velocity (kinetic energy) is related to the drop hammer's lifting height and mass as well as the boat model's weight.
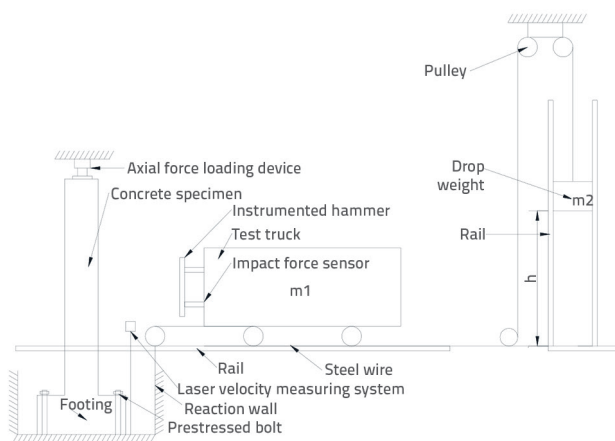
The pier specimens were placed on a rigid support and secured using four prestressing bolts, which can be approximated as a rigid connection to the support. The upper end of the column was subjected to an axial pressure of 250 kN using a hydraulic jack mounted on a reaction frame beam, as shown in Figure 7. The drop hammer was raised to the design height after installing the RC pier specimen, with the steel strand rope connected to the impact hammer tightened during this process. During the test, the drop hammer is released, which pulls the boat model to impact the specimens at different speeds. In the bottom and middle areas of the specimens, 20 measuring points were uniformly selected along the height direction of each specimen, with a grid with a side length of 5 cm selected at each measuring point to improve the measurement accuracy, as illustrated in Figure 8. For all tests conducted in this study, the impact point was 1100 mm above the base of the column. The height and position of the impact point were equivalent designs in accordance with the positions and distributions of the known impact forces in ship–bridge collisions.

2.3. Data collection

The tests were designed to investigate the damage mechanisms and dynamic responses of the two sets of RC pier models under lateral impact loads, with an American NI data-acquisition system used to collect data on the impact force, displacement, and reinforcement strain responses of the specimens. A Savitzky–Golay filter was used to reduce the dynamic data acquisition. The filtering method is based on local polynomial least-squares fitting in the time domain, which can filter noise and ensure that the shape and width of the signal remain unchanged simultaneously, making it suitable for dynamic time-history data processing. With more detailed instructions, the horizontal displacement response of the specimen was measured by the KTC-200 displacement sensor with a range

Figure 5. Multi-functional ultra-high drop hammer impact test machine system

Figure 6. CAF protection material on the test vehicle

Figure 7. Impacted specimens and constraint conditions

Figure 8. Test areas of the specimens

of 200 mm. The resistance value of the steel bar strain gauge is 120 Ω. A pressure sensor installed on the head of the impact trolley was used for measuring the impact force within a range of 0–6,285 kN, thus meeting the requirements for measuring large impact forces. To investigate the overall stress of the reinforcements, eight reinforcement strain gauges were arranged on the specimens, with their distribution shown in Figure 9. Four displacement meters were arranged on the back sides of the specimens at 100, 800, 1500, and 2,100 mm from top to bottom to collect the lateral displacement of the bridge piers, as illustrated in Figure 10. Displacement meters were used to collect the lateral displacement data of the RC piers. The damage to the failure areas of the RC piers was tested using a ZHC-U81 concrete ultrasonic detector.
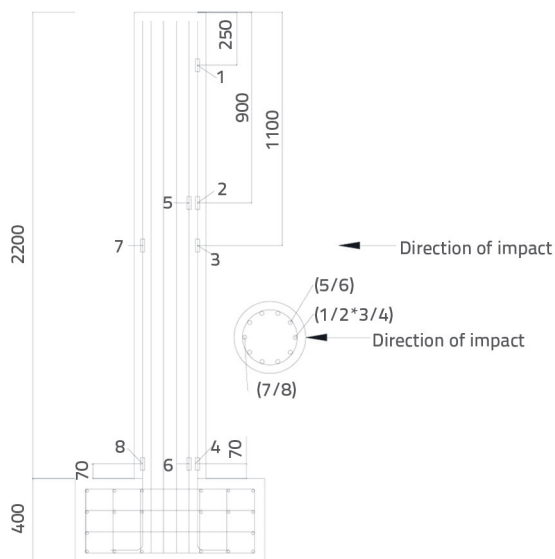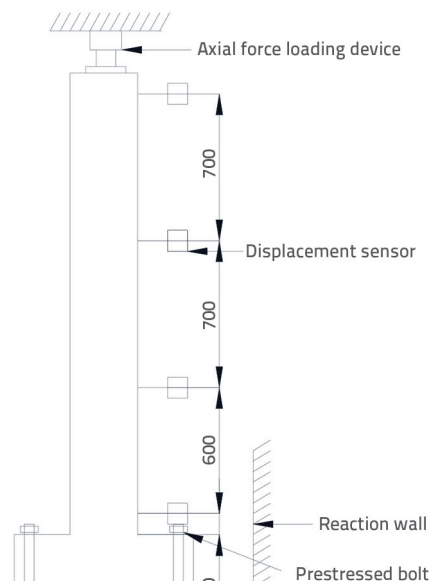

Figure 10. Diagram of the displacement measuring points (unit: mm)

2.4. Impact scheme

The experimental design included nine impacts for each pier specimen; the corresponding scheme is presented in Table 5. Based on the principle of energy conservation, the impact velocity of the theoretical boat model can be expressed as follows:

$$m_2 gh = \frac{1}{2}(m_1 + m_2)v_1^2 + \mu m_1 gh \qquad (3)$$

In Equation (3), m_1 and m_2 indicate the weights (kg) of the boat model and drop hammer, respectively; g is the acceleration of gravity (9.81 m/s²); **h** is the drop hammer's height (m); μ is the coefficient of friction between the boat model and steel rail, determined by a no-load test. In this study, for different values of m_1 and h, the friction coefficient obtained throughout testing was approximately 0.12.

Figure 9. Strain measuring point diagram of the reinforcement (dimension unit: mm)

Table 5. Pier impact scheme

Number of impacts	Height of the drop hammer [m]	Boat weight [kg]	Weight of drop hammer [kg]	Theoretical velocity [m/s]	Measured average velocity [m/s]	Velocity change rate [%]	Energy accumulation [J]
1	0.7	1200	216	0.77	0.76	1.30	606
2	1	1200	216	0.93	0.96	–3.23	1574
3	1.5	1200	216	1.14	1.14	–0.09	2939
4	2	1200	216	1.32	1.32	–0.38	4768
5	2.6	1200	216	1.50	1.54	–2.67	7258
6	3.5	1200	216	1.74	1.76	–1.15	10511
7	4.5	1200	216	1.97	1.98	–0.51	14627
8	5.5	1200	216	2.18	2.21	–1.38	19756
9	6.6	1200	216	2.39	2.43	–1.67	25956

3. Test results and analyses

The dynamic response data of RC piers protected by CAF materials of different thicknesses were obtained using horizontal impact tests. The top displacement and impact force responses of the RC piers, reinforcement strain responses, damage situations in the concerned areas of the specimens, and the derivation and propagation of cracks were analysed. Owing to the short duration of the impact, the response data for the period of interest were used to show the time-history curves for each condition. In the following analysis, 1.14 m/s, 1.76 m/s, and 2.43 m/s were selected as representative impact velocities, and the effect of the changes in the thicknesses of the CAF on the dynamic responses and damage mechanisms of the pier specimens at these impact velocities were investigated.

3.1. Response analysis of the impact force

The time-history curves when the boat model impacted the specimens at 1.14 m/s, 1.76 m/s, and 2.43 m/s, respectively, are shown in Figure 11.

According to the compression test of the CAF shown in Figure 4, the CAF stress–strain curves progressed in three stages. The first was the linear elastic stage, where the stress increased rapidly with strain and the curve was approximately straight; the second was the yield platform stage, where the volume of the CAF shrunk and the stress changed within a stable range; the last was the densification stage, where the volume of the CAF was compressed to the limit and the strain was small, but the stress increased sharply. The test results of the peak impact force of the two groups of piers were compared to further understand the
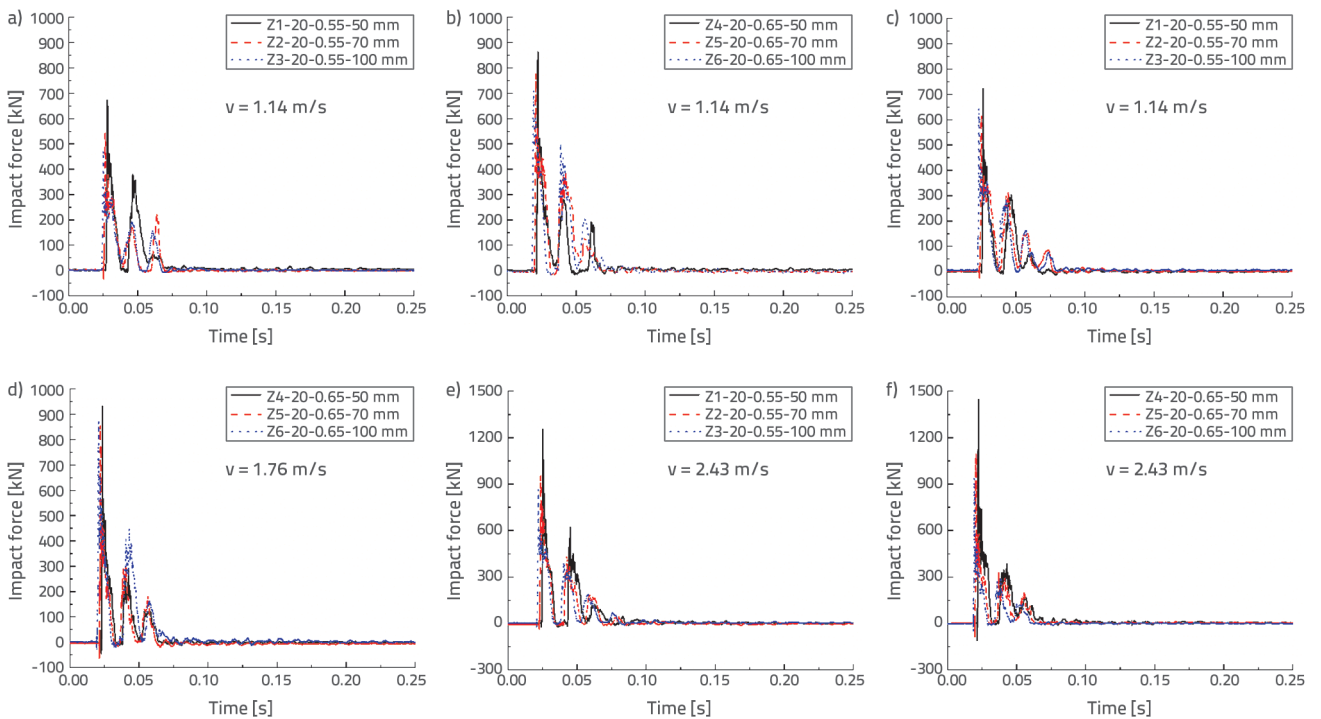

Figure 11. Time-history curves of the impact force

Table 6. Comparison of impact test results

Number of impacts	Impact velocity [m/s]	1st group			2nd group		
		Peak impact force [kN]			Peak impact force [kN]		
		Z1	Z2	Z3	Z4	Z5	Z6
1	0.76	220.33	185.19	123.84	300.91	227.77	209.52
2	0.96	482.72	349.72	291.60	681.28	561.23	490.07
3	1.14	651.58	510.44	467.99	865.21	783.56	710.98
4	1.32	664.03	559.81	518.27	872.24	798.73	742.45
5	1.54	680.48	618.14	612.65	896.25	836.63	806.94
6	1.76	701.97	619.28	643.18	932.12	860.01	880.42
7	1.98	763.25	674.10	712.28	961.25	873.60	906.45
8	2.21	961.39	764.42	811.21	1104.56	890.56	928.30
9	2.43	1223.08	929.49	835.47	1446.17	1104.67	936.92

influence of the thickness variation of the CAF materials on the peak impact force of the piers, with nine impact data points of six groups of specimens collected, as listed in Table 6.

When the impact velocity was 1.14 m/s, the cumulative impact energy was 2,939 J, with all CAFs in the yield plateau stage. As shown in Figures 11.a and 11.b, the peak value of the impact force of the pier specimens decreased with an increase in the protective thickness of the CAF. When the thickness of the CAF decreased from 50 to 75 mm, the peak force decreased by 9.44 % and 21.66 % in the first and second groups, respectively. When the thickness of the CAF increased from 75 mm to 100 mm, the peak force decreased by 8.32 % and 9.26 % in Groups 1 and 2, respectively. Compared to the 50 mm thickness, the peak force of the CAF at 100 mm showed an apparent difference. The peak forces of the first and second groups of CAF specimens decreased by 28.18 % and 17.83 %, respectively. In addition, under the same thickness condition, the density of CAF increased from 0.55 g/cm³ to 0.65 g/cm³, and the peak impact force increased by 29.49–39.43 %. Therefore, the above analysis led to the following conclusions: 1. Under the same density conditions, the peak impact force gradually decreased with an increase in the thickness of the CAF compared with that of the 50 mm thick protection; 2. For the same thicknesses and densities, the protective effects of the aluminium foam material with a higher density were reduced because the rigidity of the CAF material with a higher density is slightly higher than that of the CAF material with a lower density. When the impact velocity was 1.76 m/s, the cumulative impact energy was 10,511 J. As shown in Figures 11.c and 11.d, after a certain number of cumulative impacts, the peak impact force fluctuated in a small range with the change in the protective thickness of the CAF. After three types of CAF protection with increased thickness, the peak impact force of the first group decreased by 11.78 % and -3.86 %, whereas that of the second group decreased by 7.74 % and -2.37 %. Under the protection of the 100 mm CAF compared to the 50 mm CAF, the peak force of the two groups decreased by 8.38 % and 5.55 %, respectively. A comparison of the above results shows that the elasticity of the pier deteriorates after a certain amount of damage occurs, thus indicating that the effects of the CAF were not always better with the added thickness and that excessive thickness levels could even increase the impact force of the pier specimens. When the impact velocity was 2.43 m/s, the cumulative impact energy reached 23,956 J, and the CAF materials entered the densification stage. As shown in Figure 11.e and 11.f, the amplitudes of the impact forces of specimens Z1 and Z4 were significantly higher than those of specimens Z2, Z3, Z5, and Z6. These results indicate that the CAF with a thickness of 50 mm entered the densification stage earlier and decreased the plastic deformations and increased the rigidity, resulting in a gradual loss of its cushioning effects. Consequently, the impact force on
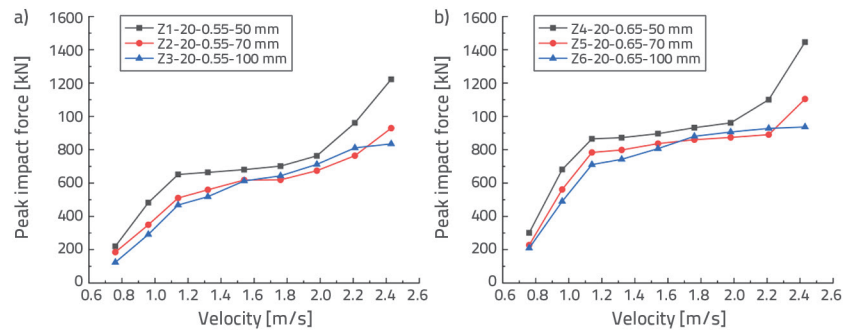

Figure 12. Peak impact force–velocity curves

the specimens could not be reduced. Furthermore, the impact force of the two groups of specimens continued to decrease by an average of 12.65 % when the thickness of the CAF was increased from 75 to 100 mm, suggesting that the 100-mm-thick CAF material was superior in reducing the impact force under large impact energy accumulation conditions.

The two groups of measured impact force peak values and impact velocities listed in Table 6 were fitted to the impact force–velocity curves, as shown in Figure 12.

In general, as shown in Figure 12 and Table 6, with an increase in the impact velocity, the trends of the impact force changes in the two specimen groups were approximately the same, with a three-stage phenomenon observed. During the first stage, when the impact velocity increased from 0.76 m/s to 1.14 m/s, the maximum impact force increased approximately linearly with an increase in impact velocity because the CAF material was still in the linear elasticity stage and exhibited weak energy-dissipation effects in that state. During the second stage, the maximum values of the impact force remained relatively steady as the impact velocity increased in the range of 1.14 m/s to 1.98 m/s, attributed to the CAF entering its yield platform stage at this time, during which it displayed its best energy consumption ability and could absorb the impact energy in an approximately constant stress state. However, when the impact velocity of the two groups of specimens reached 1.98 m/s and 2.21 m/s, respectively, the broken line in the diagram indicates that the CAF material had entered the third stage owing to the impact of energy accumulation and the CAF shifting from the yield platform stage to the densification stage.

During the densification stage, the energy-absorption capacity of the CAF material decreased rapidly. In conclusion, the three stages of impact force changes were consistent with the stress–strain curves obtained by the quasi-static uniaxial compression tests of the CAF, as shown in Fig. 4.

3.2. Displacement response analysis results

To show the changes in the lateral displacement response of the RC piers with the protection of CAF of different thicknesses, the top displacements of the piers were selected as representatives for analysing the comparison results of the displacement changes of the piers under impact loads. When
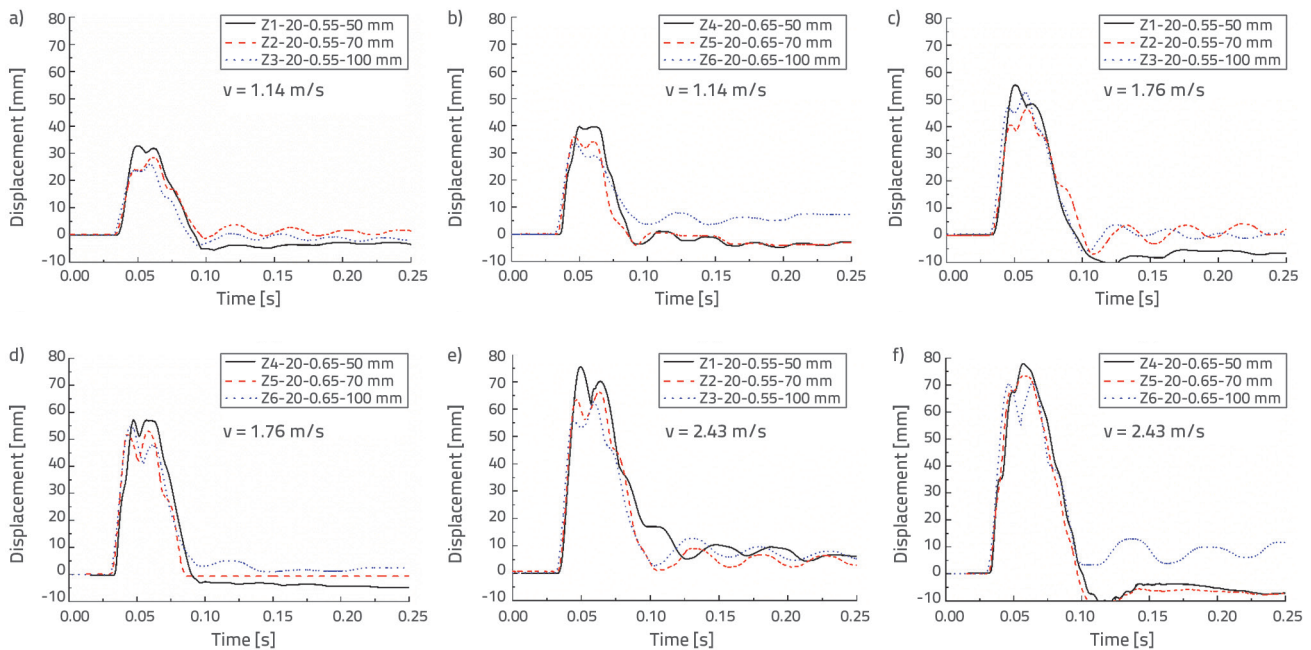
Figure 13. Time-history curves of the top displacements

the impact velocities were 1.14 m/s, 1.76 m/s and 2.43 m/s, the time-history curves for the top displacements of two specimen groups are shown in Figure 13.

When the impact velocity reaches 1.14 m/s, the peak displacement of the pier specimens decreases as the protective thickness of the CAF increases. As shown in Figures 13(a) and (b), when the thickness of the CAF in the first group increased from 50 to 75 mm, its displacement decreased by 6.16 mm (17.75 %). When the thickness of CAF increases from 50 mm to 100 mm, its displacement decreases by 8.83 mm (25.44 %). When the thickness of CAF increases from 75 mm to 100 mm, its displacement decreases by 2.67 mm (9.35 %). The results for the second group of specimens were similar, but the range of displacement change was slightly smaller. Notably, under the same thickness conditions, the density of the CAF increases from 0.55 g/cm³ to 0.65 g/cm³, while the peak displacement increases by 9.45 % to 12.21 %. Therefore, according to the calculation results of the displacement peak values of the RC piers with the protection of the CAF at three thicknesses, appropriate increases in the CAF thicknesses were conducive to reducing the displacement responses of the RC piers. However, no major differences were observed in the decreasing amplitudes of the reduced rates with increasing CAF thickness, indicating that the displacement response of the RC piers could be optimised to an ideal range by reasonably selecting the CAF thickness.

When the impact speed reaches 1.76 m/s and when the thickness of CAF material increases from 50 mm to 75 mm, the displacement decreases of the first group of specimens and the second group of specimens are 9.18 mm and 4.83 mm, respectively, decreasing by 16.57 % and 8.47 % (Figures 13.c and 13.d). When the thickness of specimens increases from 75 mm to 100 mm, the displacement reduction of specimens in the first and second groups is -6.25 mm and -2.53 mm, respectively, representing decreases of

-13.52 % and -4.85 %, respectively. According to the above data, the displacement peak values of the Z3 and Z6 pier specimens protected by CAF material with a thickness of 100 mm were higher than those of the Z2 and Z5 RC piers protected by 75 mm thick CAF material. For example, the displacements of the first group increased by 13.54 %, while the displacements of the second group increased by 4.85 %. These results further suggest that the increasing thickness of the CAF material increases the response to displacement at the tops of the RC piers.

When the impact velocity reaches 2.43 m/s, the analysis of Figure 13.e and 13.f shows that the peak values of the top displacement in the first specimen group (Z1-20, Z2-20, and Z3-20) were 74.97 mm, 65.68 mm, and 62.61 mm, respectively. The peak values of the top displacements in the second group of specimens (Z4-20, Z5-20, and Z6-20) were 79.20 mm, 73.96 mm, and 70.74 mm, respectively. Therefore, these results suggest that the peak values of the displacements of Z3 and Z6 pier specimens protected by the 100-mm-thick CAF material were lower than the top displacement peak values of the Z2 and Z5 pier specimens protected by the 75-mm-thick CAF. In summary, when the CAF thickness increased from 75 to 100 mm, the displacements of the two groups of samples decreased by 4.51 %. Thus, these results indicate that the lateral displacement responses of the piers could be better controlled using a thicker CAF under the conditions of large impact energy.

3.3. Reinforcement strain analysis results

The strain response of reinforcements in pier specimens with different thicknesses under CAF protection was analysed using the No. 7 reinforcement strain curve on the back of the pier impact point as a representative. Figure 14 shows the strain time-history curves of two specimen groups at the impact velocities of 1.14 m/s, 1.76 m/s, and 2.43 m/s.
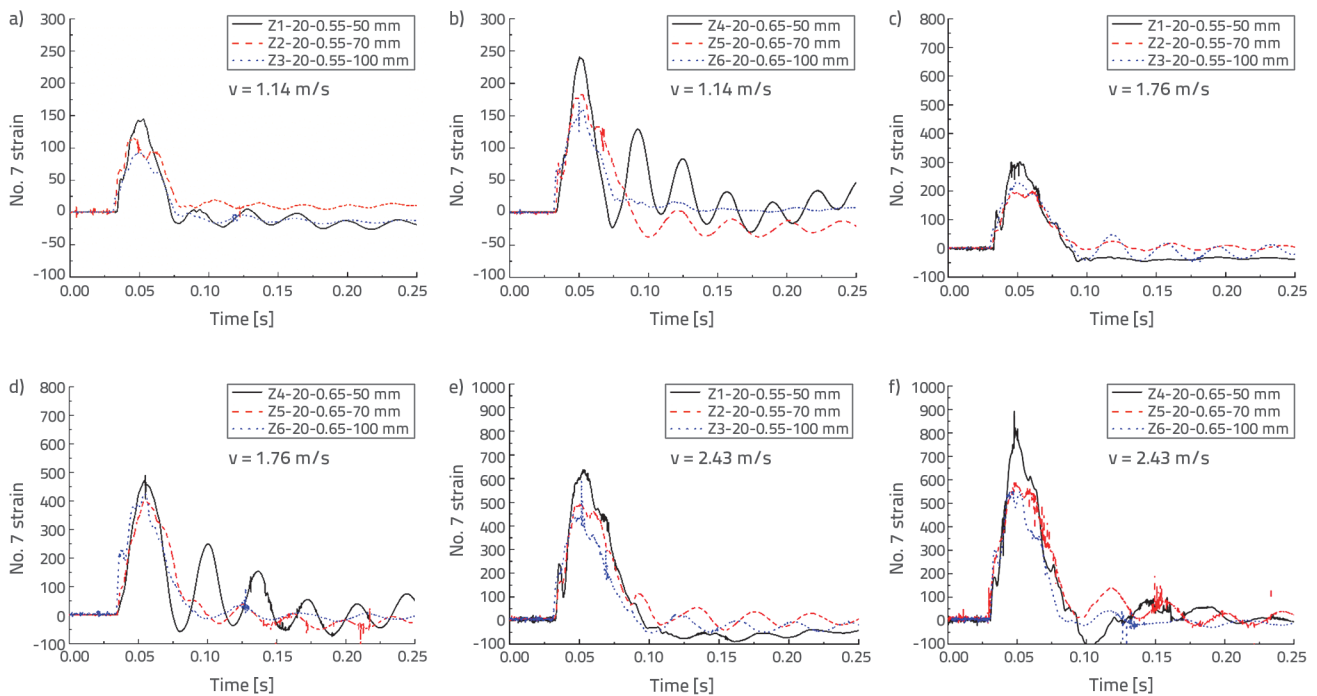
Figure 14. Time-history curves of the strain at the No. 7 reinforcement observation point

Figures 14.a and 14.b show the strain response of No.7 reinforcements located behind the impacted points of the pier specimens with changes in thickness under CAF protection at an impact velocity of 1.14 m/s. The strain peaks of the reinforcements at observation point 7 decreased with an increase in the thickness of the CAF protective material. For example, when the thickness of the CAF increased from 50 to 75 mm, the peak strain values of the two groups of specimens decreased by an average of 21.56 %. However, when the thickness increased from 75 to 100 mm, the peak values of the strain decreased on average by only 16.87 %. These results indicate that appropriate increases in the thickness of the CAF protective material are beneficial for reducing the reinforcement strain responses of the pier specimens.

Figures 14 (c) and (d) illustrate the strain response of No. 7 reinforcements located behind the impacted points of the pier specimens with changes in thickness under CAF protection. As shown in Figure 14, the reinforcement strain peak values of pier specimens Z3 and Z6 protected by a CAF with a thickness of 100 mm are higher than those of pier specimens Z2 and Z5 protected by a CAF with a thickness of 75 mm. Therefore, the above results show that the strain levels of the two groups of specimens increased by 10.09 % when the thickness of the CAF increased from 75 to 100 mm, indicating that under the condition of a certain impact energy, an excessive thickness of the CAF increased the response of the reinforcement strain of the RC piers, resulting in negative effects.

Figures 14.e and 14.f show a detailed comparison of the strain response of the No. 7 reinforcements located behind the impacted points of the pier specimens with changes in thickness under CAF protection at an impact velocity of 2.43 m/s. As illustrated in Figure 14, the reinforcement strain peak values of the Z1 and

Z4 pier specimens with the protection of the 50 mm thick CAF material were higher than those of the steel bars when the impact velocity was 1.76 m/s. When the thickness of the CAF increased from 50 to 75 mm, the reinforcement strain of the two groups of specimens decreased by 26.07 % on average. Moreover, when the thickness increased from 75 to 100 mm, the reinforcement strain decreased by an average of 7.14 %, further indicating that the CAF material with small thicknesses lost its cushioning ability under the effects of cumulative impacts. However, CAF materials with large thicknesses could still control the response of the reinforcement strain of the RC piers.
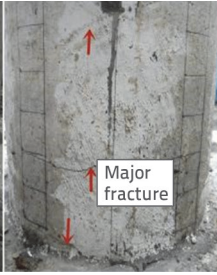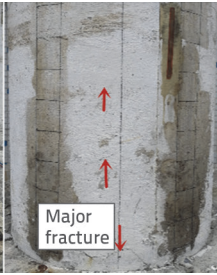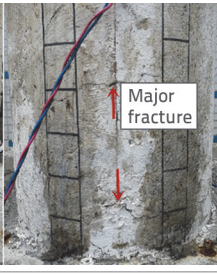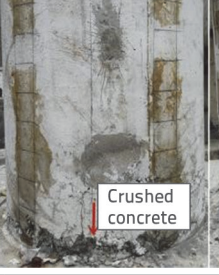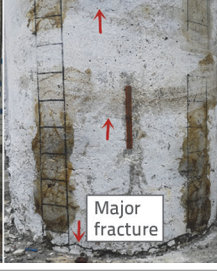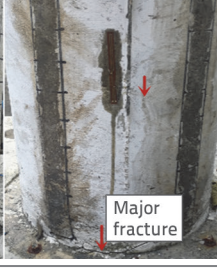
3.4. Fracture generation and failure mode analysis

The final damage degrees of the high-damage areas (pier bottom areas and areas near the impact points) of each specimen following cumulative impacts are listed in Table 7.

In Table 7, the left and right frontal areas represent areas below the sides of the impacted points. As illustrated in Table 7, different levels of lateral bending cracks were present in the bottom areas located in front of the impacted points of the two groups of piers. In addition, part of the concrete crushing action appeared in the bottom areas located behind the impacted points. In the first group of specimens, 45° oblique cracks were observed in areas located below the sides of the impacted point of the Z3 pier in the first group of specimens; similarly, 45° oblique cracks were observed in areas located below the sides of the impacted point in the second group of specimens.

The crack propagation table shows that cracks initially began to develop in the bottom areas of the impacted surfaces. Large cracks appeared at locations near the base of the RC piers when the

Table 7. Cracks in the high-damage areas of the piers

Group	Specimen	Left side of impact point	Front bottom of impact point	Rear bottom of impact point	Right side of impact point
1st group	Z1-20		Major fracture	Crushed concrete	
	Z2-20		Major fracture	Crushed concrete	
	Z3-20		Major fracture	Crushed concrete	
2nd group	Z4-20		Major fracture	Crushed concrete	
	Z5-20		Major fracture	Crushed concrete	
	Z6-20		Major fracture	Crushed concrete	

impact velocity increased to a certain level. Specimens Z1, Z2, and Z4 protected by the 50 mm and 75 mm thick CAF material only experienced cracks at the bottom front areas, with the distributions of these cracks similar to that of the cracks in the RC beams during bending failure. Therefore, when combined with the yields of concrete at the bottom of the impacted points and the evidence of concrete crushing at the bottom of the specimens, specimens Z1, Z2, and Z4 were considered to undergo bending failure. Meanwhile, the Z3 and Z5 specimens and the Z6 specimen protected by the 75 mm and 100 mm thick CAF material, respectively, displayed 45° oblique cracks in the areas located to the left and right of the impacted points. These cracks extended obliquely from the areas near the impacted points to the bottom of the piers and were similar to typical shear cracks. Therefore, according to the crack propagation table, shear cracks appear after bending cracks and develop slowly. Consequently, specimens Z3, Z5, and Z6 were considered to undergo bending-shear failures.

In accordance with the analysis results of the first group of specimens, the fracture widths of the Z1 and Z2 specimens under the same energy impact conditions were 0.64 mm and 0.35 mm, respectively, suggesting that the development of concrete cracks in RC piers could be effectively slowed down by increasing the thickness of CAF within an appropriate range. However, compared with the Z2 and Z3 specimens, as the thicknesses of the CAF were increased from 75 mm to 100 mm, the specimens' crack widths expanded from 0.35 mm to 0.56 mm. When the impact velocity reached 2.21 m/s, the Z3 specimen protected by CAF material with a thickness of 100 mm displayed oblique cracks. These results indicate that the thickness changes of the CAF affected the development of crack widths in the specimens and changed the failure modes of the RC piers under the same impact energy. The results for the second group of piers revealed that the development of the main cracks in the front areas of the piers was similar to that of the first group. However, shear cracks appeared in the RC piers when the CAF thickness increased from 50 mm to 75 mm. Hence, the excessive density of the second group of piers protected by the CAF was considered to negatively impact their protection ability.

3.5. Damage analysis of the pier concrete

The changes in the acoustic parameters of the specimens after damage were measured using an ultrasonic damage detector, as listed in Table 8. After the specimens were damaged, the propagation paths of the ultrasonic waves changed and became shorter, owing to the presence of cracks, increasing the propagation time of the ultrasound-reflected as a reduction in the speed of sound. During the experimental tests conducted in this study, the overall damage to the RC piers was evaluated using the average of the values measured at 40 points in high-damage areas [40-42].

The results in Table 8 indicate a certain regularity in the variation in the speed of sound. For example, as the impact velocity increases, the wave speed is progressively smaller, while the reduction in wave speed tends to increase as the impact velocity increases. In the present study, the first group of pier specimens was successfully analysed. When the impact velocity reached 1.32 m/s, the cumulative reductions in sound velocity for specimens Z1, Z2, and Z3 were 0.096, 0.071, and 0.059 km/s, respectively. The cumulative reduction in the sound velocity decreased when the thickness of the CAF increased, indicating that an increase in the CAF thickness under impact energy conditions reduced the damage to the RC pier specimens. A comparison of the change rates of the sound velocities of specimens Z2 and Z3 by 9.03 % and 10.99 %, respectively, indicated that the degree of concrete damage of specimen Z3 was higher than that of specimen Z2 when the impact velocity reached 2.43 m/s. Therefore, under the impact effects of that energy, the increase in the thickness of the CAF from 75 to 100 mm was considered to have damaged the concrete specimens, consistent with the development law of cracks, which indicates that excessive CAF thicknesses could adversely affect the pier specimens. The analysis results of the second group of pier specimens indicated that the concrete damage trend of the specimens as the thickness of the CAF increased was similar to that of the first group.

Table 8. Variations in ultrasonic velocities in high-damage areas of concrete piers

Group	Specimen	Impact velocity [m]	Average sound velocity [km/s]		Total reduction of sound velocity [km/s]	Change rate of sound velocity [%]
			Before impact	After impact		
1st group	Z1-20	0.76	4.208	4.199	0.672	15.97
		0.96	4.199	4.183		
		1.14	4.183	4.155		
		1.32	4.155	4.112		
		1.54	4.112	4.05		
		1.76	4.05	3.958		
		1.98	3.958	3.867		
		2.21	3.867	3.699		
		2.43	3.699	3.536		

Table 8. Variations in ultrasonic velocities in high-damage areas of concrete piers- continuation

Group	Specimen	Impact velocity [m]	Average sound velocity [km/s]		Total reduction of sound velocity [km/s]	Change rate of sound velocity [%]
			Before impact	After impact		
1st group	Z2-20	0.76	4.04	4.032	0.365	9.03
		0.96	4.032	4.018		
		1.14	4.018	4.001		
		1.32	4.001	3.969		
		1.54	3.969	3.925		
		1.76	3.925	3.877		
		1.98	3.877	3.828		
		2.21	3.828	3.777		
		2.43	3.777	3.675		
	Z3-20	0.76	4.102	4.097	0.451	10.99
		0.96	4.097	4.084		
		1.14	4.084	4.069		
		1.32	4.069	4.043		
		1.54	4.043	4.00		
		1.76	4.00	3.924		
		1.98	3.924	3.845		
		2.21	3.845	3.747		
		2.43	3.747	3.651		
2nd group	Z4-20	0.76	4.178	4.157	1.136	27.19
		0.96	4.157	4.097		
		1.14	4.097	4.024		
		1.32	4.024	3.891		
		1.54	3.891	3.761		
		1.76	3.761	3.611		
		1.98	3.611	3.455		
		2.21	3.455	3.266		
		2.43	3.266	3.042		
	Z5-20	0.76	4.1	4.084	0.853	20.80
		0.96	4.084	4.054		
		1.14	4.054	4.012		
		1.32	4.012	3.941		
		1.54	3.941	3.84		
		1.76	3.84	3.754		
		1.98	3.731	3.599		
		2.21	3.599	3.457		
		2.43	3.457	3.247		

Table 8. Variations in ultrasonic velocities in high-damage areas of concrete piers- continuation

Group	Specimen	Impact velocity [m]	Average sound velocity [km/s]		Total reduction of sound velocity [km/s]	Change rate of sound velocity [%]
			Before impact	After impact		
2nd group	Z6-20	0.76	4.131	4.118	0.921	22.29
		0.96	4.118	4.092		
		1.14	4.092	4.062		
		1.32	4.062	4.005		
		1.54	4.005	3.891		
		1.76	3.891	3.749		
		1.98	3.749	3.597		
		2.21	3.597	3.414		
		2.43	3.414	3.21		

4. Conclusions

In this study, two groups of ordinary RC piers protected by CAF materials of different thicknesses were compared and studied. The horizontal impact tests were repeated many times for the specimens, and the dynamic responses, including the impact forces, displacements, reinforcement strain, cracks, and concrete damage under horizontal impact conditions, were analysed. The CAF materials were placed in different stages of collapse by adjusting the impact velocity and were studied separately. The following conclusions were drawn from this study:

- During the first stage, with the impact velocity within 0.76–1.14 m/s, the CAF material was in the linear elastic stage and the energy dissipation of the CAF was weak in this state. Appropriate increases in the thickness of the CAF reduced the impact responses of the pier specimens. The strain change rates of the reinforcements and ultrasonic damage change rates of the specimens were observed to be small. In general, the impact effects and corresponding dynamic changes in the two specimen groups were approximately the same during the first stage.
- During the second stage, the CAF material would enter the yield platform stage, wherein the impact velocity ranged from 1.14 m/s to 1.98 m/s. The best energy dissipation effects were observed during this stage: the CAF could absorb impact energy in a near-constant stress state. The strain change rates of the reinforcement and the ultrasonic damage rates of the concrete were found to increase. An excessive increase in CAF thickness increased the reinforcement strain and peak impact force.
- During the third stage, wherein the impact speed ranged from 1.98 m/s to 2.21 m/s, the broken-line diagram displayed clear changes, indicating that the CAF material finally entered the densification stage. The impact forces in both groups increased significantly. The top displacements and concrete ultrasonic damage change rates of the specimens in the two groups were high, increasing the dynamic responses of the RC structures. Moreover, when the impact energy increased, the CAF material with a larger thickness could better control the lateral dynamic responses of the piers.
- With the increase in the density of the CAF material from 0.55 g/cm³ to 0.65 g/cm³, the protective effects of the piers were weakened. For example, when the maximum impact force increased to 29.49–39.43 %, the peak values of the displacements increased by 9.45–12.21 %, and the ultrasonic damage change rates of the RC piers increased significantly.

In conclusion, this study determined that selecting an appropriate thickness of the CAF according to the expected impact energy is crucial when it is used as a material for protecting RC piers. Appropriate CAF thicknesses were conducive to controlling the dynamic responses of the RC pier specimens subjected to impact loading. However, excessive thicknesses tend to weaken or even reduce the protective effects owing to increased structural integrity. This experimental study provides a reference for applying CAF to impact protection and other aspects of bridge structures.

In addition, research on CAF in this study is still in the experimental stage. Considering the high-efficiency energy absorption, light weight, and good durability of CAF, their application in bridge structures offers considerable development prospects. Currently, CAF materials are mainly used to protect vehicles and military facilities, while applications of CAF materials to protect bridges and other building structures remain limited. Combining CAF materials with existing anti-collision systems to develop practical components suitable for bridge protection is key to popularising CAF in civil engineering.

Acknowledgments

REFERENCES

[1] Goerlandt, F., Kujala, P.: On the reliability and validity of ship do ship collision risk analysis in light of different perspectives on risk. Science Direct, 62 (2014), pp. 348-365.

[2] Zhi-Bin, H., Qi-Zh,i L.: Review and prospect of the ship-bridge collision force, Journal of Foshan University (Natural Science Edition), 25 (2007) 5, pp. 35-39.

[3] Hua, Jm, Jun-Jie, W.: Comments on Vessel Collision Force Protection for American Highway Bridges Determined According to Risk Method[J], World Bridges, (2008) 4, pp. 64-67.

[4] Gholipour, G., Zhang, C., Mousavi, A.A.: Nonlinear numerical analysis and progressive damage assessment of a cable-stayed bridge pier subjected to ship collision, Marine Structures, 69 (2020), pp. 102662.

[5] Gholipour, G., Zhang, C., Li, M.: Effects of soil do pile interaction on the response of bridge pier to barge collision using energy distribution method, Structure and Infrastructure Engineering, (2018), pp. 1-15.

[6] Wu, M., Jin, L., Du, X.: Dynamic responses and reliability analysis of bridge double-column under vehicle collision, Engineering Structures, (2020) 221, pp. 1110-1135.

[7] Gucuyen, E., Kantar, E., Erdem, R.T., et al.: Experimental and Numerical Investigation of Steel Sections under Impact Effect, GRADEVINAR, 73 (2021) 1, pp. 45-56, https://doi.org/10.14256/JCE.2876.2020

[8] Erdem, R.T., Kantar, E., Gucuyen. E., et al.: Experimental study on hollow section joints under impact loading, GRADEVINAR, 72 (2020) 5, pp. 401-410, https://doi.org/10.14256/JCE.2776.2019

[9] Zhou, X., Zhang, R., Zhao, K., et al.: An experimental study of impact performance of RC piers with different reinforcement ratios, GRADEVINAR, 71 (2019) 6, pp. 465-479, https://doi.org/10.14256/JCE.2305.2018

[10] Erdem, R.T., Gucuyen, E.: Non-linear analysis of reinforced concrete slabs under impact effect, GRADEVINAR, 69 (2017) 6, pp. 479-487, https://doi.org/10.14256/JCE.1557.2016

[11] Erdem, R.T., Gucuyen, E., Kantar, E., et al.: Impact behaviour of concrete beams, GRADEVINAR, 66 (2014) 6, pp. 523-531, https://doi.org/10.14256/JCE.1034.2014

[12] Tkalčević Lakušić, V.: Safety of roadside columns in case of vehicle impact, GRAĐEVINAR, 64 (2012) 4, https://doi.org/10.14256/JCE.652.2011

[13] Jing-You, C., Cheng-Bing, L.l.: Study Progress in Mechanical Properties and Energy Absorption Characteristic of Aluminum Foams, Development and Application of Materials, 4 (2013) 21, pp. 1003-1545.

[14] Mu, Y.L., Wang, D.D., He, Y.D., et al.: Impact Toughness of Closed-Cell Aluminum Foam, Materials Science Forum, (2018) 933, pp. 203-208.

[15] Shan, C.L., Xu, X.J.: Analysis of mechanical properties of pier anti-collision device by sandwich plate 520 with overall curved surface, Zhongguo Gonglu Xuebao/China Journal of Highway and Transport, 52127 (2014) 10, pp. 46-54.

[16] Yang, Y.S., Zhe, Y., et al.: Study on the cushioning property and deformation failure mechanism of close-cell aluminum foam , Journal of Functional Materials, 45 (2014) 8.

[17] Shi, S.Q., Kang, J.G., Sui, S.B.: Experimental Study of Quasi-static and Dynamic Compressive Property of Close-cell Aluminum Foam, Rare Metal Materials and Engineering, (2011) s2, pp. 150-154.

[18] Gibson, L.J., Ashby, M.F.: CellularSolids: Structure and Properties, Cambridge University Press, (1997), pp. 203-208.

[19] Yu, H.J., Li, B., Guo, Z.Q., et al.: Dynamic compressive property of closed-cell aluminum foam with Al matrix and Al-6Si matrix, Zhongguo Youse Jinshu Xuebao/Chinese Journal of Nonferrous Metals, 17 (2007) 5, pp. 704-709.

[20] Reyes, G.: Static and Low Velocity Impact Behavior of Composite Sandwich Panels with an Aluminum Foam Core, Journal of Composite Materials, 42 (2008) 16, pp. 1659-1670.

[21] Li, X., Li, Z., Zhang, D.: Mechanical Behaviors of Closed-Cell Aluminum Foams under Quasi-Static Compression-Shear Loads, Gaoya Wuli Xuebao/Chinese Journal of High Pressure Physics, 32 (2018) 3.

[22] Shakibanezhad, R., Sadighi, M., Hedayat,i R:. Numerical and Experimental Study of Quasi-Static Loading of Aluminum Closed-Cell Foams Using Weaire-Phelan and Kelvin Tessellations, Transport in porous media, 142 (2022) 1-2, pp. 229-248.

[23] Li, Z.B., Li, X.Y., Zheng, Y.X.: Biaxial mechanical behavior of closed-cell aluminum foam under combined shear-compression loading, Transactions OF Nonferrous Metals Society OF China, 30 (2020) 1, pp. 41-50.

[24] Li, B.C., Zhao, G.P., Lu, T.J.: Low strain rate compression behavior of high porosity closed-cell aluminum foams,Chinese Journal of Theoretical and Applied Mechanics, 43 (2011), pp. 122-135.

[25] Sun, G., Wang, E., Zhang, J., et al.: Experimental study on the dynamic responses of foam sandwich panels with different facesheets and core gradients subjected to blast impulse, International Journal of Impact Engineering, (2019) 135, pp. 103327.

[26] Wang, E., Li, Q., Sun, G.: Computational analysis and optimization of sandwich panels with homogeneous and graded foam cores for blast resistance, Thin-Walled Structures, (2020) 147, pp. 106494.

[27] Huo, X., Sun, G., Zhang, H., et al.: Experimental study on low-velocity impact responses and residual properties of composite sandwiches with metallic foam core, Composite Structures, (2019) 223(SEP.), pp. 110835.1-110835.20.

[28] Sun, G., Wang, E., Wang, H., et al.: Low-velocity impact behaviour of sandwich panels with homogeneous and stepwise graded foam cores, Materials & Design, (2018) 160(DEC.), pp. 1117-1136.

[29] Liu, J., Wu, C., Li, C., et al.: Blast testing of high performance geopolymer composite walls reinforced with steel wire mesh and aluminium foam, Construction and Building Materials, (2019) 197, pp. 533-547.

[30] Xia, Y., Wu, C., Liu, Z.X., et al.: Protective effect of graded density aluminium foam on RC slab under blast loading-an experimental study, Construction and Building Materials, (2016) 111, pp. 209-222.

[31] Lin, Y., Shun-Feng, G., Wei-Liang, J.: Investigation on anti-explosion performance of reinforced concrete slab with composite protective aluminum foam, Journal of Zhejiang University (Engineering Science), 43(2009) 2, pp. 376-379.

[32] Zhu, C.: Dynamic response and damage mechanism of reinforced concrete structures under 562 crash, Tianjin: Tianjin University, 2012.

[33] Gao, H., Liu, Z., Yang, Y., Wu, C., Geng, J.: Blast-resistant performance of aluminum foam-protected reinforced concrete slabs, Explosion Andshock Waves, 39 (2019) 2, pp. 30-41.

[34] Wu, Y., He, S.M., Li, X.P., et al.: Study on elliptic anti rock-fall impact structure with double energy dissipation layers wrapping up pier eccentrically in mountains, Engineering Mechanics, 34 (2017) 10, pp. 158-167.

[35] Zulie, W.U.T.: Experimental Research of Pier with Foam Aluminum Protection Devices, Structural Engineers, 25 (2009) 3, pp. 125-130.

[36] Xu, D.F.: Application of Aluminum Foam Protection Device in Bridge Pier Collision Avoidance, Chongqing, Jiaotong University, Chongqing, China, 2006.

[37] Zhou, X., Zhang, W., Wang, X., et al.: Experimental Study on the Impact Resistance of Closed-Cell Aluminum Foam Protective Materials to RC Piers under Lateral Impact, Advances in Materials Science and Engineering, 2021.

[38] Zhou, X., Zhang, H., Zhang, W., et al.: Study on the Influence of Closed-Cell Aluminum Foam on the Impact Performance of Concrete Pier after Equal Replacement with Stainless Steel Reinforcement, Advances in Materials ence and Engineering, (2020) 19, pp. 1-17.

[39] Li, Q., Magkiriadis, I., Harrigan, J.: Compressive strain at the onset of densification of cellular solids, 568 Cell. Plast, 42 (2006) 5, pp. 371-392.

[40] Sellitto, A., Riccio, A., Russo, A., et al.: Ultrasonic Damage Detection of Impacted Long and Short Fibre Composite Specimens, Key Engineering Materials, (2020) 827.

[41] Shirole, D., Hedayat, A., Ghazanfari, E., et al.: Evaluation of an Ultrasonic Method for Damage Characterization of Brittle Rocks, Rock Mechanics and Rock Engineering, 4 (2020).

[42] Patil, S., Reddy, D.M.: Impact damage assessment in carbon fiber reinforced composite using vibration-based new damage index and ultrasonic C-scanning method, Structures, 28 (2020), pp. 638-650.